Slow slip rate and excitation efficiency of deep low-frequency tremors beneath southwest Japan

Slow slip rate and excitation efficiency of deep low-frequency tremors beneath southwest Japan

Kumiko Daiku, Graduate School of Natural Science and Technology, Kanazawa University, Kanazawa, 920-1192, Japan, e-mail: kumidai130@gmail.com

Yoshihiro Hiramatsu, School of Natural System, College of Science and Engineering, Kanazawa University, Kanazawa, 920-1192, Japan, e-mail: yoshizo@staff.kanazawa-u.ac.jp

Takanori Matsuzawa, National Research Institute for Earth Sciences and Disaster Resilience, Tsukuba, Japan, e-mail: tkmatsu@bosai.go.jp

Tomoyuki Mizukami, School of Natural System, College of Science and Engineering, Kanazawa University, Kanazawa, 920-1192, Japan, e-mail: peridot@staff.kanazawa-u.ac.jp

Corresponding author: Yoshihiro Hiramatsu

Key words: slow slip event; slip rate; serpentinite; pore fluid pressure; Nankai Trough

Abstract

We estimated the long-term average slip rate on the plate interface across the Nankai subduction zone during 2002–2013 using deep low-frequency tremors as a proxy for short-term slow slip events based on empirical relations between the seismic moment of short-term slow slip events and tremor activities. The slip rate in each region is likely to compensate for differences between the convergence rate and the slip deficit rate of the subducting Philippine Sea plate estimated geodetically, although the uncertainty is large. This implies that the strain because of the subduction of the plate is partially stored as the slip deficit and partially released by slow slip events during the interseismic period. The excitation efficiency of the tremors for the slow slip events differs among regions: it is high in the northern Kii region. Some events in the western Shikoku region show a somewhat large value. Antigorite serpentinite of two types exists in the mantle wedge beneath southwest Japan. Slips with more effective excitation of tremors presumably occur in high-temperature conditions in the antigorite + olivine stability field. Other slip events with low excitation efficiency are distributed in the antigorite + brucite stability field. Considering the formation reactions of these minerals and their characteristic structures, events with high excitation efficiency can be correlated with a high pore fluid pressure condition. This result suggests that variation in pore fluid pressure on the plate interface affects the magnitude of tremors excited by slow slip events.

1. Introduction

In southwest Japan, the Philippine Sea (PHS) plate subducts beneath the Eurasian plate. Great earthquakes occur with a 100–150 year recurrence interval at the Nankai trough (e.g. Ando, 1975). Deep slow earthquakes, including nonvolcanic deep low-frequency (DLF) tremors (Obara, 2002), short-term slow slip events (SSE) (Obara et al., 2004), and very low-frequency earthquakes (Ito et al., 2007) occurring on the plate interface in southwest Japan have been reported from measurements obtained using dense seismic and geodetic networks throughout Japan. In southwest Japan, DLF tremors accompany short-term SSEs on the plate interface of the PHS plate (e.g., Obara et al., 2004). Such a spatiotemporal correlation, which has also been reported in Cascadia, is designated as an episodic tremor and slip (ETS) (Rogers and Dragert, 2003). Previous reports of some studies have described a proportional relation of ETS events between the moment of short-term SSEs observed geodetically and the size of DLF tremors as the apparent moment from the reduced displacement (Hiramatsu et al., 2008), duration (Aguiar et al., 2009), and number (Obara, 2010).

Monitoring of the slip at the ETS zone is important to elucidate the seismogenic process of interplate major earthquakes because DLF tremors and short-term SSEs take place at the deeper extension of such great earthquake source areas. Gao and Wang (2017) proposed a thermo-rheological model of slip behavior for ETS zones. In their model, the ETS zone is not a monotonic spatial transition of seismic to aseismic frictional behavior, but is instead controlled by the thermo-petrological condition in the mantle wedge corner. They showed that the ETS zone is separated from

58 the mega-thrust earthquake zone in the Nankai subduction zone, suggesting that the neighboring
59 creep drives episodic slips at the ETS zone. DLF tremors can be a proxy for short-term SSEs because
60 minor tremor episodes of short duration are often observed with undetectable SSEs by geodetic
61 observations because of the lack of a sufficient number of stations to capture the crustal deformation
62 (Obara and Hirose, 2006). Hiramatsu et al. (2008) proposed an empirical procedure to estimate the
63 long-term average slip rate attributable to short-term SSEs at the ETS zone on the plate interface
64 from DLF tremors. Applying this method, the average slip rate has been estimated in the subduction
65 zone along the Nankai trough. In Shikoku and the Kii Peninsula, the average slip rate is
66 approximately consistent with differences between the convergence rate and the slip deficit rate of
67 the subducting PHS plate (Hirose et al., 2010b; Ishida et al., 2013).
68 In the southern Kii Peninsula, however, Ishida et al. (2013) reported that the slip rate
69 differed significantly from the difference between the convergence rate and the slip deficit rate. They
70 suggested that this discrepancy resulted from the lateral variation in the proportional relation between
71 the sizes of DLF tremors and SSEs, or the existence of a steady or quasi-steady slip. Yabe and Ide
72 (2014) reported a heterogeneous distribution of the sizes of tremors defined by the band-limited
73 seismic energy rate, and pointed out that the proportional relation between the sizes of DLF tremors
74 and SSEs does not always hold.
75 Previous studies have used short-term SSEs data, observed by tiltmeters operated by the
76 National Research Institute for Earth Science and Disaster Resilience (NIED) (Sekine et al., 2010) to

77 estimate the average slip rate. Recently, Nishimura et al. (2013) detected short-term SSEs using
78 Global Navigation Satellite System (GNSS) data. Their catalog includes SSEs that are undetectable
79 to a tiltmeter. They reported that short-term SSEs might be undetected by both methods.
80 Observations of SSEs conducted with multiple geodetic sensors are necessary to elucidate SSE
81 characteristics.
82 This study re-estimated the long-term average slip rate at the ETS zone on the plate interface by
83 re-analyzing DLF tremors and using short-term SSEs detected by tiltmeters and the GNSS.
84 Subsequently, we assess the relation between the re-estimated average slip rate, the convergence rate,
85 and the slip deficit rate of the PHS plate at the ETS zone. We also report heterogeneity of the size of
86 DLF tremors excited by short-term SSEs and discuss the relation to mineral assemblages, antigorite
87 serpentinite of two types, at the ETS zone.
88
89 **2. Data and method**
90
91 We analyzed waveform data recorded by a nationwide high-sensitivity seismograph network
92 (Hi-net) operated by NIED, during April 2002 – July 2013 in the Tokai region, the Kii Peninsula and
93 the Shikoku region of southwest Japan. We used hypocenter catalogs of DLF tremors determined
94 using the hybrid method (Maeda and Obara, 2009) and the hybrid clustering method (Obara et al.,
95 2010). The former is a method that combines the envelope correlation method (Obara, 2002) with

96 spatial distributions of amplitude data, assuming tremor locations at the plate interface estimated by
97 Shiomi et al. (2008). The latter catalog is processed using a clustering technique to estimate centroid
98 locations and to eliminate non-tremor sources from the hybrid method. We used the former catalogue
99 for visual checking of waveform data of DLF tremors and the latter one for tremor location.
100 We divided belt-like distributions of DLF tremors in the Kii Peninsula and the Shikoku
101 region, respectively, into three segments bounded by the low-activity zones of DLF tremors: the
102 northern, central, and southern areas of the Kii Peninsula (Ishida et al., 2013); and the eastern,
103 central, and western areas of the Shikoku region (Hirose et al., 2010b) (Fig. 1). For this analysis, we
104 selected Hi-net stations, which provide high S/N waveform data of DLF tremors, in each region. We
105 used the Hi-net stations ASHH, ASUH, HOUH, STRH, and TDEH in the Tokai region (Hiramatsu et
106 al., 2008); HYSH, KAWH, and TKWH for the northern area, and HNZH, TKEH, and TKWH for the
107 central and southern areas of the Kii Peninsula (Ishida et al., 2013); and SINH, SADH, and IKWH
108 for the eastern area, and IKKH, SJOH, and GHKH for the central area, and HITH, KWBH, OOZH,
109 TBEH, and IKKH for the western area of the Shikoku region (Hirose et al., 2010b) (Fig. 1a). We also
110 used 62 SSEs estimated from the NIED Hi-net tiltmeter data (Sekine et al., 2010; NIED, 2014) and
111 68 SSEs estimated from the GNSS data (Nishimura et al., 2013) (Fig. 1b). Some SSEs, but not
112 others, were detected from both the tiltmeter and GNSS data. The numbers of SSEs detected by
113 either or both the tiltmeter and GNSS in each region are presented in Table 1. For SSEs observed by
114 both tiltmeter and GNSS, we used their average seismic moment. We corrected the seismic moment

115 of SSEs observed by either tiltmeter or GNSS to fit the trend of the average seismic moment.

116 We estimated the seismic moment of the slip on the plate interface from DLF tremors
117 following the empirical procedure proposed by Hiramatsu et al. (2008). First, we calculated the root-
118 mean-square (RMS) amplitude of the vertical component for ground displacement by application of a
119 band-pass filter of 2–10 Hz, integrating velocity waveform by time, and a moving average with a
120 time window of 6 s. We define a DLF tremor event as follows: (1) the start time of a tremor is the
121 time at which the RMS amplitude becomes larger than the noise level; (2) the end time of a tremor is
122 the time at which the RMS amplitude becomes smaller than the noise level; (3) the duration is > 1
123 min; and (4) the maximum RMS amplitude is greater than twice the noise level. Next, we convert the
124 observed amplitudes to reduced displacements (D_{RQ}), which are the RMS amplitudes corrected for
125 geometrical spreading and inelastic attenuation, although previous works applied correction for
126 geometrical spreading only. We calculated D_{RQ} as $D_{RQ} = A \cdot r \cdot exp(\pi f_c Q^{-1} t_i)$ (m^2), where A
127 represents the RMS amplitude, r stands for the distance between the tremor source and the receiver,
128 f_c signifies the center frequency, Q^{-1} denotes the intrinsic attenuation factor, and t_i is the travel
129 time from the tremor source to the receiver. An intrinsic attenuation factor $Q = 184$ is also used
130 (Maeda and Obara, 2009). We set the center frequency $f_c = 6$ (Hz) from a 2–10 Hz band-pass filter.
131 In addition, we estimate the apparent moment as the event size of DLF tremors from the average of
132 the time integral of the D_{RQ} amplitude at each station assuming the envelope of D_{RQ} as the
133 apparent moment rate function (Hiramatsu et al., 2008). We calculate the sum of the apparent

134 moment of an episode of the DLF tremors excited by a corresponding short-term SSE.

135 We used short-term SSEs observed geodetically. Then we estimated the conversion factor
136 from the apparent moment of DLF tremors to the seismic moment of SSEs in each region. After
137 obtaining the conversion factor, we can estimate the seismic moment of the SSE from multiplication
138 of the conversion factor by the apparent moment of DLF tremors, even if the event is not detected
139 geodetically (Hiramatsu et al., 2008; Hirose et al., 2010b; Ishida et al., 2013). Figure 2 presents the
140 relation between the seismic moment of SSEs observed geodetically and the cumulative apparent
141 moment of a corresponding episode of DLF tremors. In estimating the conversion factor, because
142 SSEs propagate over two segmentations between the seven areas we set, we divided the study areas
143 into five regions: Tokai, northern Kii, central and southern Kii, eastern Shikoku, and central and
144 western Shikoku. For this study, we combined several episodes that are subdivided to express the
145 migration of the slip area in the SSE catalog of NIED.

146 We estimated the conversion factor using the non-parametric bootstrap method. The size of
147 the bootstrap sample is the same as that of the original data. The standard error and 95% confidence
148 range were calculated from 2000 bootstrap estimations. The conversion factors, shown as the slopes
149 in Fig. 2, are $5.3 \pm 1.1\ (3.7 - 8.1) \times 10^{16}\ \mathrm{N/m/s}$ in the Tokai region, $3.0 \pm 0.3\ (2.5 - 3.7) \times$
150 $10^{16}\ \mathrm{N/m/s}$ in the northern Kii region, $4.9 \pm 0.4\ (4.4 - 5.8) \times 10^{16}\ \mathrm{N/m/s}$ in the central and
151 southern Kii region, $7.0 \pm 0.7\ (5.8 - 8.4) \times 10^{16}\ \mathrm{N/m/s}$ in the eastern Shikoku region, and
152 $5.1 \pm 0.5\ (4.2 - 6.1) \times 10^{16}\ \mathrm{N/m/s}$ in the central and western Shikoku region, where values after

153 ± and in parentheses respectively represent the standard error and the 95% confidence range (Table
154 2).

155 In earlier studies, the conversion factor of the Kii Peninsula was estimated using SSEs
156 detected in the northern area (Ishida et al., 2013). That of the Shikoku region was estimated using
157 SSEs detected in the western area (Hirose et al., 2010b) because SSEs were rarely observed in the
158 central and southern Kii region or the eastern Shikoku region during the analysis periods. For this
159 study, the conversion factor in the central and southern Kii regions is estimated as larger than that in
160 the northern area. The conversion factor in the eastern Shikoku region is apparently larger than that
161 in the central and western Shikoku regions, although the 95% confidence range overlaps slightly. The
162 variation in these values and the widely various uncertainties, reflecting the scatter of data presented
163 in Fig. 2, of the conversion factors might reflect variation in the frictional properties on the plate
164 interface in each region. We discuss this point in Section 4.

165

166 **3. Average slip rate estimated from DLF tremors**

167

168 Fig. 3 presents the temporal variation in the cumulative seismic moment, at the ETS zone on
169 the plate interface during the analysis period, as estimated from DLF tremors and the conversion
170 factor. The steady increase in the cumulative seismic moment provides the long-term average rate of
171 the moment release attributable to short-term SSEs on the plate interface. We can estimate the

172 average slip rate. Table 2 presents the estimated seismic moment release rates in each region.

173 In addition, Fig. 3 shows that the cumulative seismic moment of SSEs detected geodetically
174 is smaller than that estimated from DLF tremors. The rates of the seismic moment of the geodetically
175 undetected SSEs are approximately 40%, 30%, 90%, 50%, and 55%, respectively, in the Tokai,
176 northern Kii, central and western Kii, eastern Shikoku, and central and western Shikoku regions. The
177 rate of the entire Nankai subduction zone is estimated as approximately 55%. We show the size–
178 frequency distribution of SSEs detected geodetically in the Nankai subduction zone in two ways in
179 Fig. 4: exponential and power-law distributions. We used here the average and corrected seismic
180 moment described above as the size of the SSEs. Fig. 4 shows the lack of detection capability of the
181 SSEs detected geodetically below the seismic moment of around 1.0×10^{18} Nm. Therefore, we
182 calculated the best-fit line in Fig. 4 from data greater than 1.0×10^{18} Nm for each distribution. If
183 we were able to observe smaller SSEs, as expected by the extrapolation of the best-fit line of the
184 exponential distribution, then the cumulative seismic moment of geodetically detected SSEs would
185 be close to that estimated from DLF tremors. However, extrapolation of the power-law distribution
186 gives a much larger cumulative seismic moment, which implies that the size distribution of short-
187 term SSEs is approximated by an exponential distribution rather than by a power law distribution, as
188 reported by Hirose et al. (2010b).

189 To estimate the slip rate $\dot{U}$ at the ETS zone from the moment release rate $\dot{M}_o$, we used the
190 formula $\dot{M}_o = \mu \dot{U} S$, where S is the fault area related to the slip of short-term SSEs in each region

and μ is the rigidity (Hiramatsu et al., 2008). We approximate that the fault area is equal to the active area of DLF tremors as follows. We set 3 km $\times$ 3 km blocks on the plate interface and projected on the surface with a dip of 20°, which is the average dip of source faults of short-term SSEs observed geodetically. Then we counted blocks in which the number of the epicenters of DLF tremors was greater than five. We calculated the area on the plate interface from the number of such blocks. The estimated fault areas in each region are shown in Table 2. Assuming rigidity of 40 GPa (Hiramatsu et al., 2008; Hirose et al., 2010b; Ishida et al., 2013), we obtain average slip rates of $2.0 \pm 0.4\ (1.4 - 3.0)$ cm/year in the Tokai region; $2.5 \pm 0.3\ (2.0 - 3.0)$ cm/year, $3.3 \pm 0.3\ (2.9 - 3.9)$ cm/year, and $3.8 \pm 0.3\ (3.4 - 4.5)$ cm/year, in the northern, central, and southern Kii regions, respectively; $3.9 \pm 0.4\ (3.2 - 4.6)$ cm/year, $2.6 \pm 0.2\ (2.1 - 3.1)$ cm/year, and $4.5 \pm 0.4\ (3.8 - 5.4)$ cm/year in the eastern, central, and western Shikoku regions, respectively (Fig. 5 and Table 2). It is noteworthy that the standard error (values after $\pm$) and the 95% confidence range (values in parenthesis) are estimated by those of the conversion factors in each region. However, these estimations depend clearly on how the fault areas are estimated. For example, $\pm 20\%$ changes of the threshold of the number of DLF tremors per block results in $\pm 4 - 12\%$ changes of the slip rate in each area. Another factor on the uncertainty of the average slip rates is the seismic moment of SSEs. Sekine et al. (2010) reported that the uncertainty of the seismic moment of SSE was 17–77%. In addition, our dataset of SSEs includes the difference of estimations depending on the analyzed data and methods. Therefore, a considerable uncertainty of slip rate inferred from

210 that of the seismic moment of SSEs can be larger than that of the fault area.

211 The depth distribution of the slip deficit rate on the plate interface is an important parameter
212 for elucidating the seismogenic processes of great earthquakes in the subduction zone. Hirose et al.
213 (2010b) emphasized that the average slip rates estimated from DLF tremors compensate for
214 differences between the slip deficit rate at the ETS zone and the convergence rate of the PHS plate
215 beneath the Shikoku region. Ishida et al. (2013) estimated the average slip rates at the ETS zone
216 beneath the Kii Peninsula, and reported that the average slip rates are consistent with differences
217 between the slip deficit rate and the convergence rate of the PHS plate, except in the southern area of
218 the Kii Peninsula. We re-estimate the average slip rate from DLF tremors throughout southwest
219 Japan and compare the balance between these rates: the average slip rate, the slip deficit rate, and the
220 convergence rate of the PHS plate in each region.

221 The slip deficit rates are 1.5 cm/year in the Tokai region (Suito and Ozawa, 2009) ; 2.6
222 cm/year, 2.2 cm/year, and 1.0 cm/year in the northern, central, and southern Kii regions (Kobayashi
223 et al., 2006); and 2.1 cm/year, 3.4 cm/year, and 2.6 cm/year in the eastern, central, and western
224 Shikoku regions (Tabei et al., 2007). The convergence rates of the PHS plate are 3.0–4.0 cm/year in
225 the Tokai region, 5.0–6.5 cm/year in the Kii Peninsula, and 6.5–6.8 cm/year in the Shikoku region
226 (Miyazaki and Heki, 2001). The differences between the slip deficit rate and the convergence rate of
227 the subducting plate are calculated as the following: 1.5–2.5 cm/year in the Tokai region; 2.4–3.9
228 cm/year, 2.8–4.3 cm/year, and 4.0–5.5 cm/year in the northern, central, and southern areas of the Kii

229 Peninsula; and 4.4–4.7 cm/year, 3.1–3.4 cm/year, and 3.9–4.2 cm/year in the eastern, central, and
230 western areas of the Shikoku region. These values are approximately equal to the slip rates
231 attributable to short-term SSEs estimated from DLF tremors in this study, except for the central
232 Shikoku region in southwest Japan (Fig. 5), although the uncertainty of the slip rate is large (Table 2)
233 and we cannot deny the possibility of a mismatch between these quantities. We infer that the strain at
234 the ETS zone accumulated by the subduction of the PHS plate is partially stored as a slip deficit and
235 partially released by short-term SSEs in the interseismic period, except for long-term SSE periods,
236 beneath southwest Japan. The slip deficit rates cited in this study were estimated in the inter-long-
237 term SSE period. Therefore, the slip rate and the slip deficit rate averaged over much longer period
238 would be, respectively, larger and smaller.

239 Our result might resolve the inconsistency in the southern Kii region reported by Ishida et
240 al. (2013) attributable to estimation of the typical conversion factor in the central and southern Kii
241 regions because we re-analyze DLF tremors and use SSEs data detected by the GNSS in addition to
242 the tiltmeter data. This result also emphasizes the importance of along-strike variation in the
243 conversion factor for estimation of the average slip rate using the DLF tremors. In other words,
244 simple estimation of slip rate over a subduction zone based on the activity of DLF tremors provides
245 incorrect estimations. However, confirmation of this result requires more SSEs together with DLF
246 tremors. The need exists for reanalysis to obtain more reliable estimation of the conversion factor
247 and slip rate in future works.

248 In the central Shikoku region, the average slip rate we estimated might be less than the
249 difference between the convergence rate and the slip deficit rate of the PHS plate. We assumed a
250 constant conversion factor in the central and western Shikoku regions because nine SSEs share the
251 fault area in these regions and only two SSEs exist in the central Shikoku region. However, the
252 average frictional properties on the plate interface might be different in each region, implying a
253 larger conversion factor in the central Shikoku region than in the western Shikoku region. If we
254 estimate the conversion factors in the central and western Shikoku regions simultaneously using the
255 least squares method for all DLF tremors and SSEs in these regions, then we obtain conversion
256 factors of $9.7 \pm 1.7 \times 10^{16}$ N/m/s and $4.6 \pm 0.4 \times 10^{16}$ N/m/s, respectively, giving an
257 average slip velocity of 4.7 ± 0.9 cm/year and 4.1 ± 0.3 cm/year in the central and western
258 Shikoku regions. As expected, the conversion factor in the central Shikoku region is estimated as
259 larger than that in the western Shikoku region. However, the average slip rate in the central Shikoku
260 region in this case is greater than the difference between the convergence rate and the slip deficit rate
261 of the PHS plate in this region. This relation arises again from the small number of SSEs in the
262 central Shikoku region. A sufficient number of SSEs in the central Shikoku region might enable us to
263 estimate a reliable conversion factor and a slip rate in this region.
264 In the manner described above, we can estimate the conversion factors in the central and
265 southern Kii regions simultaneously using the least squares method. The obtained conversion factors
266 are $4.4 \pm 0.4 \times 10^{16}$ N/m/s and $5.7 \pm 0.6 \times 10^{16}$ N/m/s, respectively, in the central and

267 southern Kii regions. The average slip velocities are 3.0 ± 0.3 cm/year and 4.4 ± 0.5 cm/year.
268 These estimations imply a smaller conversion factor in the northern Kii region. The average slip
269 velocities estimated here are apparently coincident with the difference between the convergence rate
270 and the slip deficit rate of the PHS plate in this region. However, we emphasize that more SSEs are
271 needed in the central and southern Kii regions for reliable estimations.
272
273 **4. Heterogeneous distribution of the excitation efficiency of DLF tremors by short-term SSEs**
274
275 In Section 2, we estimated conversion factors correlating the apparent moment of DLF
276 tremors with the seismic moment of SSEs as the average values for seven regions to obtain the local
277 average slip rates in the regions. We emphasize the variation in the conversion factor of each SSE,
278 which is the ratio of the seismic moment of an SSE to the apparent moment of a coincident episode
279 of DLF tremors. First, we estimate the average value of the conversion factor over southwest Japan,
280 using all the SSEs analyzed in this study, to be $4.0 \pm 0.2 \times 10^{16}$ N/m/s by least squares fitting.
281 Next, we normalize a conversion factor for an individual SSE by the average one. Fig. 6 portrays a
282 spatial distribution of the normalized conversion factors for SSEs in southwest Japan.
283 The DLF tremors sometimes migrate with a velocity of approx. 10 km/day (e.g. Obara,
284 2002). Obara (2010) reported that tremor migration is induced by the rupture initiation of the SSE
285 because of the very sharp front of tremor migration, and sustained tremor activity behind the front.

286 Hirose and Obara (2010) estimated the slip propagation as 8–18 km/day for SSEs from time
287 evolution inversion analysis of the slip on the plate interface. The coincidence of the tremor
288 migration velocity with the slip propagation rate for SSEs indicates that the migrating tremors are
289 caused by the rupture front of the SSE. Ando et al. (2010) showed that a physical model composed of
290 heterogeneously and sparsely distributed unstable patches in a stable background can reproduce the
291 migration pattern of the DLF tremors in terms of the rupture of patches triggered by the slow slip
292 front.

293 The conversion factor represents the inverse of the excitation efficiency of DLF tremors by
294 short-term SSEs. Our results (Fig. 6) demonstrate that the excitation efficiency differs among
295 locations along the strike of the subducting PHS plate. It is particularly large in the northern Kii
296 region. In the western Shikoku region, we find some events with the excitation efficiency as high as
297 in the northern Kii region, although the scatter is large. Modification of the Q values by higher
298 (+20%) and lower (-20%) values provides a similar along-strike variation in the excitation efficiency.
299 Furthermore, we examine the effect of a heterogeneous Q structure on the spatial variation of the
300 excitation efficiency by combining the results of the reference and a higher or lower, Q value. Figure
301 7 presents the variation in excitation efficiency for cases of a higher Q only in the northern Kii region
302 (upper panels in Fig. 7) and only in the central and western Shikoku regions (lower panels in Fig. 7).
303 The results show that the spatial variation in the excitation efficiency is not altered to any remarkable
304 degree by a heterogeneous Q, although the contrast becomes weak in the western Shikoku region for

305 the cases of a lower Q in the northern Kii region and a higher Q in the central and western Shikoku
306 regions.

307 Ide and Yabe (2014) analyzed very low-frequency (0.02–0.05 Hz) (VLF) events that
308 occurred in active tremor areas in the Nankai subduction zone. They estimated the scaled energy, the
309 energy rate divided by seismic moment rate, of VLF events. They demonstrated the spatial
310 distribution of the scaled energy of VLF events, as high in the entire Kii region and low in the Tokai
311 and western Shikoku regions. The normalized conversion factors estimated in this study are low in
312 the northern Kii region. Hiramatsu et al. (2008) reported that the conversion factor is proportional to
313 the inverse of the scaled energy as a ratio of seismic moment of SSEs to radiated energy of DLF
314 tremors. Therefore, it is interesting that the spatial distribution of the scaled energy of VLF events is
315 almost coincident with that of the normalized conversion factors in spite of the difference in
316 frequency band of the analyzed events. However, in the western Shikoku region, the normalized
317 conversion factor might not be so high as expected by the inverse of the scaled energy of VLF
318 events. If this is the case in the western Shikoku region, then this fact suggests that the frequency
319 content radiated as seismic waves in a low-frequency to very low-frequency band relative to slow
320 deformation differs from that in other regions.

321 High excitation efficiency indicates that the SSE tends to excite large magnitudes of DLF
322 tremors in a slip, and vice versa. The heterogeneity in the excitation efficiency of DLF tremors by
323 SSEs might derive from inhomogeneity of frictional properties of the slip planes, probably on the

plate interface. In general, the frictional behavior of slow slip phenomena can be changed depending on the temperature conditions, the fluid amount, and the structural and rheological properties of fault gouge and rocks (Obara, 2011). What is the most likely cause for the heterogeneous tremor excitation?

DLF tremors and SSEs are regarded as occurring on the plate interface because of the high pore fluid pressure. As supporting evidence, seismic observations have revealed concentrations of fluid released from the oceanic crust of the subducting plate and/or serpentinization at the hanging wall mantle. In the Nankai subduction zone, three-dimensional seismic velocity structures presented by Matsubara et al. (2008) show high V_p/V_s zones along the distribution of DLF tremors at depths of 30 km. They suggested that DLF tremors might occur at all parts of the high V_p/V_s zone where the oceanic crust of the PHS plate encountered the serpentinized mantle wedge beneath the Eurasian plate. Shelly et al. (2007) and Kato et al. (2010) respectively reported that DLF tremors occurred along the top of a high V_p/V_s zones beneath the Shikoku and Tokai regions. Shibutani et al. (2009) and Saiga et al. (2013) also respectively reported the existence of a thin serpentinized layer on the plate interface beneath the Kii region from the receiver function and S-wave splitting analyses.

To consider the more detailed structures detected by our analyses, we particularly examine the mineral assemblages of serpentinite in the mantle wedge. Mizukami et al. (2014) discussed a possible causal relation between the characteristics of long-term and short-term slow slip behaviors in the Shikoku region, and two distinct types of antigorite serpentinite inferred in the hanging wall

343 mantle. The formation of the antigorite (Atg) + brucite (Brc) serpentinite (hydration reaction:
344 $\text{olivine} + H_2O \rightarrow \text{antigorite} + \text{brucite}$) absorbs large amounts of H_2O. It can reduce pore fluid
345 pressure, although the formation of the Atg + olivine (Ol) serpentinite (hydration reaction:
346 $\text{olivine} + H_2O + SiO_2 \rightarrow \text{antigorite} + \text{olivine}$) might generate high pore fluid pressure because
347 the reaction is controlled by the amount of SiO_2 (Mizukami et al., 2014).
348 Short-term SSEs and deep low-frequency tremors are known to be active in the down dip
349 portion of the source region of long-term SSE in the western Shikoku region. The source region for
350 the long-term SSE is inferred to form a composite structure in which slip characteristics of the plate
351 boundary change with depth. Nakata et al. (2017) fitted a two-segment model for heterogeneous slip
352 behaviors of the long-term SSEs recorded in GEONET data. This fitting is coincident with the
353 petrological model of Mizukami et al. (2014): the shallower portion of the long-term SSE region on
354 the subduction boundary is inferred to be overlain by a mantle wedge with the Atg + Brc mineral
355 assemblage. The mantle overlying the down dip portion is inferred to be near/within the Atg + Ol
356 stability. As serpentinization of mantle wedge peridotite proceeds, the hydrated mantle weakens its
357 ability to absorb slab-derived fluid. As a result, build-up of pore pressure is enhanced even in the Atg
358 + Brc stability. The hybrid slip nature will be obscured because of antigorite serpentinization of two
359 types. However, our petrological interpretation based on a recent thermal model of Nankai
360 subduction zone (Fig. 8) shows that short-term SSEs in the Atg + Brc regions are less active in terms
361 of frequency and magnitude, implying that slip planes for short-term SSE might be relatively minor

362 and sparse in Atg + Brc stability. The heterogeneous occurrence of short-term SSEs indicates that the
363 mantle beneath southwest Japan is not mature. It still affects fluid pressures in the Nankai subduction
364 zone.

365 Fig. 8 presents a phase diagram for hydrous ultramafic rocks compiled by Mizukami et al.
366 (2014). We compare the subduction geotherm of each region (Ji et al., 2016) with the petrological
367 change along the plate interface. Ji et al. (2016) estimated the thermal structure on the plate interface
368 of the PHS plate using a 3-D parallelepiped model of the subducting plate in the thermal convection.
369 Events with a high excitation efficiency in the northern Kii and western Shikoku regions occur
370 predominantly in the Atg + Ol stability field (Fig. 8). By contrast, events with a low excitation
371 efficiency occur mostly in the Atg + Brc stability field. As an exception, events in the central
372 Shikoku region, for which the excitation efficiency is low, lie in the Atg + Ol stability field (Fig. 8).
373 The configuration of the subducting PHS plate bends greatly beneath the central Shikoku region
374 (Shiomi et al., 2008). The 3D thermal simulation might not completely reproduce the effect of such
375 complexity, causing a bias of thermal conditions on the plate interface. Perhaps for this reason,
376 events in the central Shikoku region belong to the Atg + Ol stability field.

377 Magnitudes of DLF tremors detected on the surface are ascertained through propagation
378 processes of seismic waves in overlying layers as well as source processes associated with short-term
379 SSEs. The existence of brucite in mantle wedge reduces the elastic stiffness (Jian et al., 2006) and the
380 mechanical strength upon shear (Moore and Lockner, 2007). From seismological observations, it is

inferred that the tremor source is clusters of fluid-filled patches in which shear stress and pore fluid pressure are accumulated (Obara, 2011; Ando et al., 2010), and furthermore, that the fundamental structure of the tremor source may be common in the Atg + Ol and Atg + Brc regions. Important variables affecting the total moment release of DLF tremors are elastic energy in a single patch and spatial density of the patches on a slip plane of SSE and activation rate. Given that weak frictional strengths of the patches define critical shear stress to cause tremors, the variable rigidity of the wall rock mantle, that is mechanical strength, might not have marked effects on shear strain energy. Highly elevated fluid pressures reduce the effective normal stress and the fracture strength of the fault plane, and engender frequent SSE activities by stress perturbations (Obara, 2011). In this case, DLF tremors might also be excited easily by stress perturbation accompanied by short-term SSEs under high pore fluid pressure in the Atg + Ol stability field. If the collapse of fluid-filled patches is a fundamental process of tremor formation (Ando et al., 2010), then the extent of the elevation of pore pressure might be related directly to the tremor magnitude. Therefore, we suggest that the heterogeneity of the pore fluid pressure on the plate interface, induced by the phase transition of antigorite serpentinite, causes a heterogeneous distribution of the magnitude of DLF tremors excited by short-term SSEs.

5. Conclusions

After analyzing waveform data of DLF tremors recorded by Hi-net in southwest Japan, we have estimated the conversion factor from the apparent moment of DLF tremors of a corresponding episode to the seismic moment of short-term SSEs based on the proportional relation between their magnitudes. The cumulative seismic moment, as estimated from DLF tremors using the conversion factor, increases constantly over the long term and shows a steady moment release on the plate interface. We estimated the average slip rate at the ETS zone on the plate interface of the subducting PHS plate from DLF tremors. The average slip rates are apparently coincident with differences between the convergence rate and the slip deficit rate of the PHS plate, as estimated geodetically except for the central Shikoku region, although the uncertainty is large. Therefore, the short-term SSEs release the strain, except for slip deficit, accumulated through subduction of the PHS plate in the interseismic period at the Nankai subduction zone. We also investigated the spatial distribution of the conversion factor of each SSE. Actually, the conversion factor can be interpreted as the inverse of the excitation efficiency of DLF tremors by short-term SSEs. The excitation efficiency is distributed heterogeneously along the strike of the subducting PHS plate. Higher ones are distributed dominantly in the northern Kii. Slightly higher ones are also found in the western Shikoku region. We have compared the subduction geotherm beneath each region to the mineral assemblages of serpentinite in the mantle wedge. Events in the northern Kii and western Shikoku regions are predominant in the Atg + Ol assemblage, providing high pore fluid pressures. Others are predominant in the Atg + Brc assemblage. We suggest the variations in the pore fluid pressure and the mechanical strength of the

hanging wall mantle as possible causes of the difference in the magnitudes of DLF tremors excited by short-term SSEs.

Acknowledgements

We are grateful to Takuya Nishimura for providing us with short-term SSE data observed by GNSS. We thank Shoichi Yoshioka, Yingfeng Ji, and Ayako Nakanishi for providing geometry data and the thermal structure of the upper surface of the subducting Philippine Sea plate beneath southwestern Japan. Constructive comments from Suguru Yabe, Kelin Wang, and an anonymous reviewer have been useful to improve the paper. GMT software (Wessel and Smith, 1998) was used to produce all figures.

References

Aguiar, A.C., Melbourne, T.I., Scrivner, C.W., 2009. Moment release rate of Cascadia tremor constrained by GPS. J. Geophys. Res. 114, B00A05, doi:10.1029/2008JB005909.

Ando, M., 1975. Source mechanisms and tectonic significance of historical earthquakes along the Nankai Trough, Japan. Tectonophysics 27, 119–140.

438

439 Ando, R., Nakata, R., Hori, T., 2010. A slip pulse model with fault heterogeneity for low-frequency
440 earthquakes and tremor along plate interfaces. Geophys. Res. Lett. 37, L10310,
441 doi:10.1029/2010GL043056.

442

443 Gao, X., Wang, K., 2017. Rheological separation of the megathrust seismogenic zone and episodic
444 tremor and slip. Nature 543, 416–419, doi:10.1038/nature21389.

445

446 Hiramatsu, Y., Watanabe, T., Obara, K., 2008. Deep low-frequency tremors as a proxy for slip
447 monitoring at plate interface. Geophys. Res. Lett. 35, L13304, doi:10.1029/2008GL034342.

448

449 Hirose, H., Asano, Y., Obara, K., Kimura, T., Matsuzawa, T., Tanaka, S., Maeda, T., 2010a. Slow
450 earthquakes linked along dip in the Nankai subduction zone. Science 330, 1502.

451

452 Hirose, T., Hiramatsu, Y., Obara, K., 2010b. Characteristics of short-term slow slip events estimated
453 from deep low-frequency tremors in Shikoku, Japan. J. Geophys. Res. 115, B10304,
454 doi:10.1029/2010JB007608.

455

456 Hirose, H., Obara, K., 2005. Repeating short- and long-term slow slip events with deep tremor

457 activity around the Bungo channel region, southwest Japan. Earth Planets Space 57, 961–972.

458

459 Hirose, H., Obara, K., 2010. Recurrence behavior of short-term slow slip and correlated nonvolcanic

460 tremor episodes in western Shikoku, southwest Japan. J. Geophys. Res. 115, B00A21,

461 doi:10.1029/2008JB006050.

462

463 Ide, S., Yabe, S., 2014. Universality of slow earthquakes in the very low frequency band. Geophys.

464 Res. Lett. 41, 2786–2793, doi:10.1002/2014GL059712.

465

466 Ishida, R., Hiramatsu, Y., Matsuzawa, T., Obara, K., 2013. Average slip rate at the transition zone on

467 the plate interface beneath the Kii Peninsula, Japan, estimated from deep low-frequency tremors.

468 Earth Planets Space 65, 1047–1051.

469

470 Ito, Y., Obara, K., Shiomi, K., Sekine, S., Hirose, H., 2007. Slow earthquake coincident with episodic

471 tremors and slow slip events. Science 315, 503–506.

472

473 Ji, Y., Yoshioka, S., Matsumoto, T., 2016. Three-dimensional numerical modeling of temperature and

474 mantle flow fields associated with subduction of the Philippine Sea plate, southwest Japan. J.

475 Geophys. Res. 121, doi:10.1002/2016 JB012912.

476

477 Jiang, F., Speziale, S., Duffy, T.S., 2006. Single-crystal elasticity of brucite, $Mg(OH)_2$, to 15 GPa by

478 Brillouin scattering. Am. Min., 91, 1893–1900.

479

480 Kato, A., Iidaka, T., Ikuta, R., Yoshida, Y., Katsumata, K., Iwasaki, T., Sakai, S., Thurber, C.,

481 Tsumura, N., Yamaoka, K., Watanabe, T., Kunitomo, T., Yamazaki, F., Okubo, M., Suzuki, S.,

482 Hirata, N., 2010. Variations of fluid pressure within the subducting oceanic crust and slow

483 earthquakes. Geophys. Res. Lett. 37, L14310, doi:10.1029/2010GL043723.

484

485 Kobayashi, T., Hashimoto, M., Tabei, T., 2006. Estimate of interplate coupling along the Nankai

486 Trough, southwest Japan, using a new plate interface model. EOS Trans. AGU 87, S43D-7.

487

488 Maeda, T., Obara, K., 2009. Spatiotemporal distribution of seismic energy radiation from low-

489 frequency tremor in western Shikoku, Japan. J. Geophys. Res. 114, B00A09,

490 doi:10.1029/2008JB006043.

491

492 Matsubara, M., Obara, K., Kasahara, K., 2008. Three-dimensional P- and S-wave velocity structures

493 beneath the Japan Islands obtained by high-density seismic stations by seismic tomography.

494 Tectonophysics 472, 6–17, doi:10.1016/j.tecto.2008.06.013.

495

496 Miyazaki, S., Heki, K., 2001. Crustal velocity field of southwest Japan: Subduction and arc–arc

497 collision. J. Geophys. Res. 106, 4305–4326, doi:10.1029/2000 JB900312.

498

499 Mizukami, T., Yokoyama, H., Hiramatsu, Y., Arai, S., Kawahara, H., Nagaya, T., Wallis, S.R., 2014.

500 Two types of antigorite serpentinite controlling heterogeneous slow-slip behaviours of slab-mantle

501 interface. Earth and Planetary Science Letters 401, 148–158.

502

503 Moore, D.E., Lockner, D.A., 2007. Comparative deformation behavior of minerals in serpentinized

504 ultramafic rocks: Application to the slab–mantle interface in subduction zones. Inter. Geol. Rev. 49,

505 401–415.

506

507 Nakata, R., Hino, H., Kuwatani, T., Yoshioka, S., Okada, M., Hori, T., 2017. Discontinuous

508 boundaries of slow slip events beneath the Bungo Channel, southwest Japan. Sci. Rep. 7, Article

509 number: 6129, doi:10.1038/s41598-017-06185-0.

510

511 Nishimura, T., Matsuzawa, T., Obara, K., 2013. Detection of short-term slow slip events along the

512 Nankai Trough, southwest Japan, using GNSS data. J. Geophys. Res. 118, 3112–3125,

513 doi:10.1002/jgrb.50222.

514

515 Obara, K., 2002. Nonvolcanic Deep Tremor Associated with Subduction in Southwest Japan. Science

516 296, 1679–1681.

517

518 Obara, K., 2010. Phenomenology of deep slow earthquake family in southwest Japan:

519 Spatiotemporal characteristics and segmentation. J. Geophys. Res. 115, B00A25.

520

521 Obara, K., 2011. Characteristics and interactions between non-volcanic tremor and related slow

522 earthquakes in the Nankai subduction zone, southwest Japan. J. Geodyn. 52, 229–248.

523

524 Obara, K., Hirose, H., 2006. Non-volcanic deep low-frequency tremors accompanying slow slips in

525 the southwest Japan subduction zone. Tectonophysics 417, 33–51, doi:10.1016/j.tecto.2005.04.013.

526

527 Obara, K., Hirose, H., Yamamizu, F., Kasahara, K., 2004. Episodic slow slip events accompanied by

528 non-volcanic tremors in southwest Japan subduction zone. Geophys. Res. Lett. 31, L23602,

529 doi:10.1029/2004GL020848.

530

531 Obara, K., Tanaka, S., Maeda, T., Matsuzawa, T., 2010. Depth-dependent activity of non-volcanic

532 tremor in southwest Japan. Geophys. Res., Lett. 37, L13306, doi:10.1029/2010GL043679.

533

534 Ozawa, S., Murakami, M., Kaidzu, M., Tada, T., Sagiya, T., Hatanaka, Y., Yarai, H., Nishimura, T.,

535 2002. Detection and monitoring of ongoing aseismic slip in the Tokai region, central Japan. Science

536 298, 1009–1012.

537

538 Rogers, G., Dragert, H., 2003. Episodic tremor and slip on the Cascadia subduction zone: The chatter

539 of silent slip. Science 300, 1942–1943.

540

541 Saiga, A., Kato, A., Kurashimo, E., Iidaka, T., Okubo, M., Tsumura, N., Iwasaki, T., Sakai, S., Hirata,

542 N., 2013. Anisotropic structures of oceanic slab and mantle wedge in a deep low-frequency tremor

543 zone beneath the Kii Peninsula, SW Japan. J. Geophys. Res. 118, 1091–1097.

544

545 Sekine, S., Hirose, H., Obara, K., 2010. Along-strike variations in short-term slow slip events in the

546 southwest Japan subduction zone. J. Geophys. Res. 115, B00A27, doi:10.1029/2008 JB006059.

547

548 Shelly, D.R., Beroza, G.C., Ide, S., 2007. Non-volcanic tremor and low frequency earthquake

549 swarms. Nature 446, 305–307, doi:10.1038/nature05666.

550

551 Shibutani, T., Hirahara, K., Ueno, T., 2009. Receiver function analyses for estimating seismic
552 velocity discontinuity structure. Zishin 2 (J. Seismol. Soc. Jpn.) 61, 199–207 (in Japanese with
553 English abstract).

554

555 Shiomi, K., Matsubara, M., Ito, Y., Obara, K., 2008. Simple relationship between seismic activity
556 along Philippine Sea slab and geometry of oceanic Moho beneath southwest Japan. Geophys. J. Int.
557 173, 1018–1029, doi:10.1111/j.1365-246X.2008.03786.x.

558

559 Suito, H., Ozawa, S., 2009. Transient crustal deformation in the Tokai District –The Tokai Slow Slip
560 Event and Postseismic deformation caused by the 2004 off southeast Kii Peninsula earthquake.
561 Zishin 2 (J. Seismol. Soc. Jpn.) 61, 113–135. (in Japanese with English abstract)

562

563 Tabei, T., Adachi, M., Miyazaki, S., Watanabe, T., Kato, S., 2007. Interseismic deformation of the
564 Nankai subduction zone, southwest Japan, inferred from three-dimensional crustal velocity fields.
565 Earth Planets Space 59, 1073–1082.

566

567 Wessel, P., Smith, W.H.F., 1998. New improved version of Generic Mapping Tools released. EOS
568 Trans. AGU 79, 579.

569

570 Yabe, S., Ide, S., 2014. Spatial distribution of seismic energy rate of tectonic tremors in subduction

571 zones. J. Geophys. Res. 119, 8171–8185, doi: 10.1002/2014JB011383.

572 **Figure captions**

573

574 **Fig. 1.** (a) Distribution of DLF tremors in southwest Japan. Dots show epicenters of DLF tremors
575 (Obara et al., 2010). Triangles show Hi-net stations used for this study. The analysis area is divided
576 into three segments in the Kii Peninsula and the Shikoku region, respectively, shown by rectangles
577 with thick lines. (b) Dark gray and light gray rectangles respectively show locations of the fault
578 models of SSEs observed by tiltmeter and GNSS.

579

580 **Fig. 2.** Relation between the seismic moment of short-term SSEs observed geodetically and the
581 cumulative apparent moment of the corresponding episode of DLF tremors. Dotted, solid, and
582 dashed lines respectively present the best-fit lines for the data in the Tokai region, Kii Peninsula, and
583 Shikoku region.

584

585 **Fig. 3.** Temporal variation in the cumulative apparent moment (left axis) and in the seismic moment
586 (right axis) from DLF tremors (red line). The light green and blue lines and arrows respectively
587 indicate the cumulative seismic moment and the occurrences of SSEs observed by tiltmeter and
588 GNSS. Pink hatched zones show SSEs observed by both tiltmeter and GNSS. Gray hatched zones
589 show the period of long-term SSEs in Tokai (Ozawa et al., 2002; Suito and Ozawa, 2009), and in the
590 Bungo channel (Hirose and Obara, 2005; Hirose et al., 2010a).

591

592 **Fig. 4.** Size–frequency distribution of geodetically detected SSEs: (a) exponential distribution and

593 (b) power-law distribution. The solid line shows the best-fit line for data greater than

594 1.0×10^{18} Nm. R^2 is the coefficient of determination of the fitting.

595

596 **Fig. 5.** Average slip rates at the ETS zone on the plate interface estimated from DLF tremors in

597 southwest Japan. Solid and open red arrows respectively indicate the slip rates attributable to short-

598 term SSEs estimated from DLF tremors in this study and in previous studies (Hirose et al., 2010b;

599 Ishida et al., 2013). Black arrows indicate the slip deficit rates at the ETS zone on the plate interface

600 of the subducting PHS plate from the Nankai Trough (Tabei et al., 2007; Kobayashi et al., 2006;

601 Suito and Ozawa, 2009). Blue arrows show the convergence rates of the PHS plate (Miyazaki and

602 Heki, 2001).

603

604 **Fig. 6.** Distribution of the normalized conversion factors of each SSE by the average one estimated

605 from all SSEs in southwest Japan depicted in Fig. 3. Circles and thick lines respectively portray the

606 central points and the upper edges of the fault plane of SSEs. The dashed lines represent depth

607 contours of the oceanic Moho discontinuity (Shiomi et al., 2008).

608

609 **Fig. 7.** Distributions of the normalized conversion factors of each SSE by the average one estimated

610 from all SSEs for heterogeneous Q structures, with lower (-20%) and higher (+20%) Q values in the
611 northern Kii region and in the central and western Shikoku regions. All symbols are the same as
612 those presented in Fig. 5.
613
614 **Fig. 8.** (a) Phase diagram of serpentinite (modified from Mizukami et al., 2014). The dashed curves,
615 which correspond to the lines in Fig. 6b, indicate the temperature structure beneath southwest Japan.
616 The stars show high-activity areas of tremors and SSEs in each region. (b) Red curves show
617 isotherms of the upper surface of the PHS plate (Ji et al., 2016).
618
619 **Table 1.** Summary of the number of SSEs, as detected with either or both the tiltmeter and GNSS
620 data, in each region used for this study.
621
622 **Table 2.** Results for estimation of the average slip rate and each rate of the subducting PHS plate in
623 the Tokai, northern Kii, central Kii, southern Kii, eastern Shikoku, central Shikoku, and western
624 Shikoku regions. Values after ± and in parentheses respectively represent the standard error and the
625 95% confidence range.
626

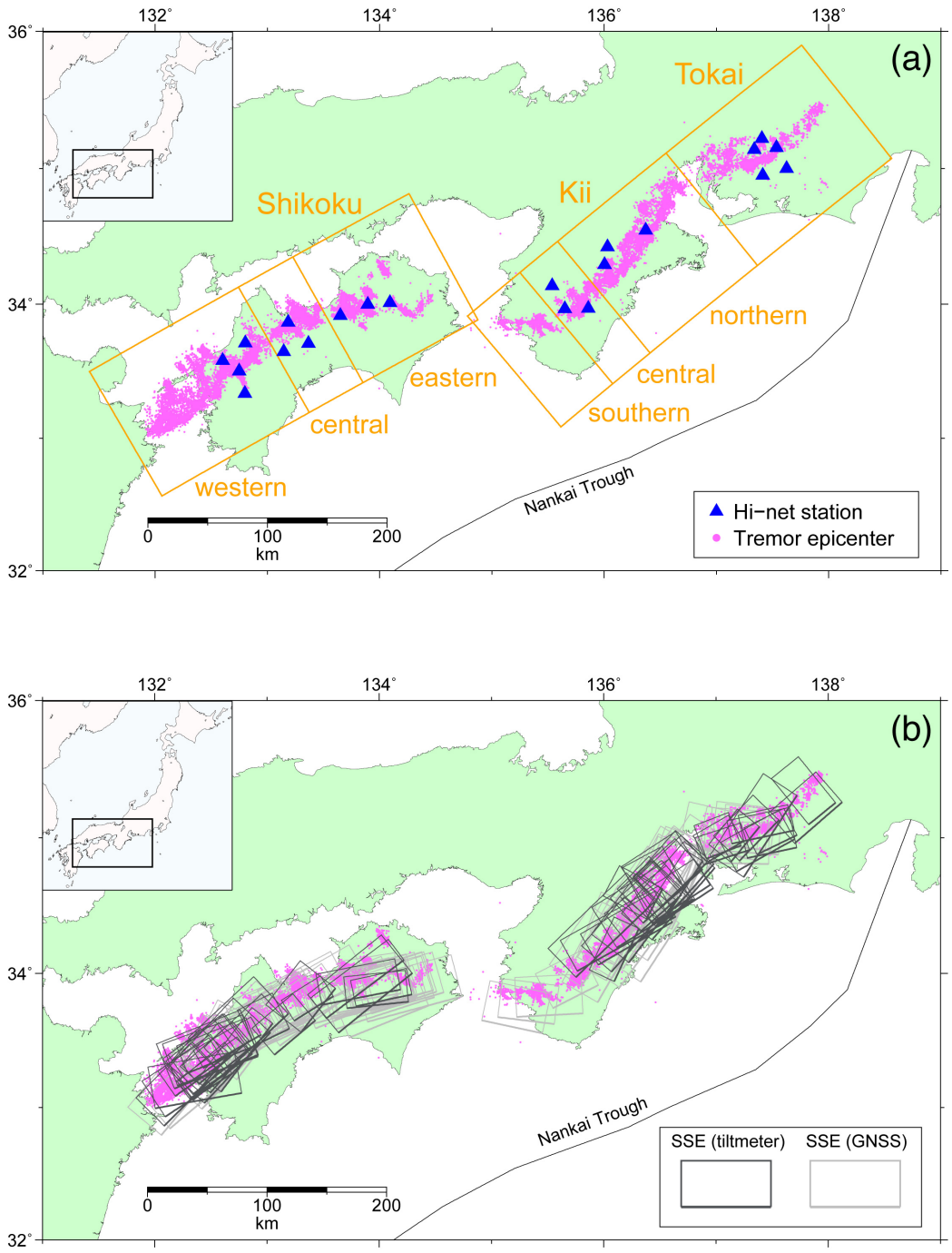

627
628
629 Figure 1.
630
631

632

633

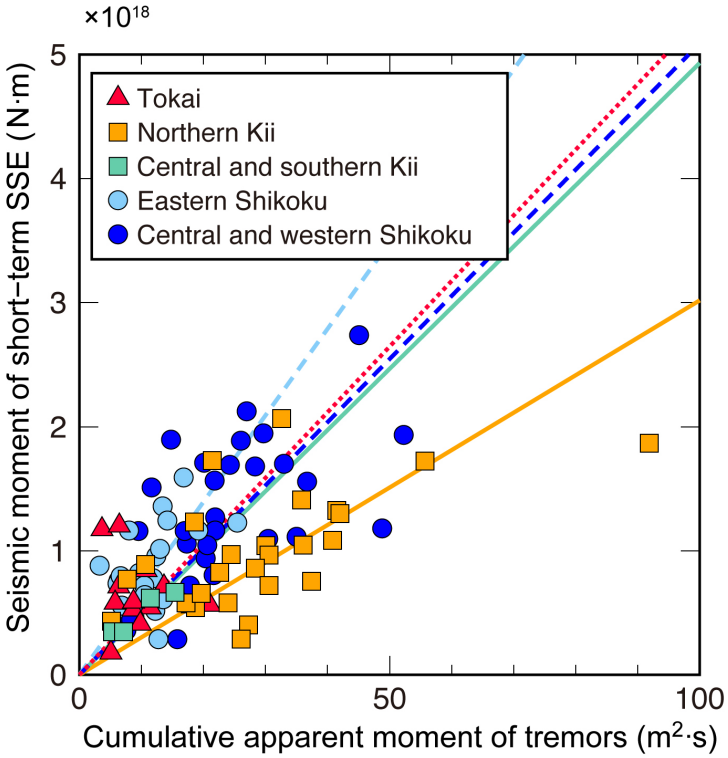

634

635 Figure 2.

636

637

638

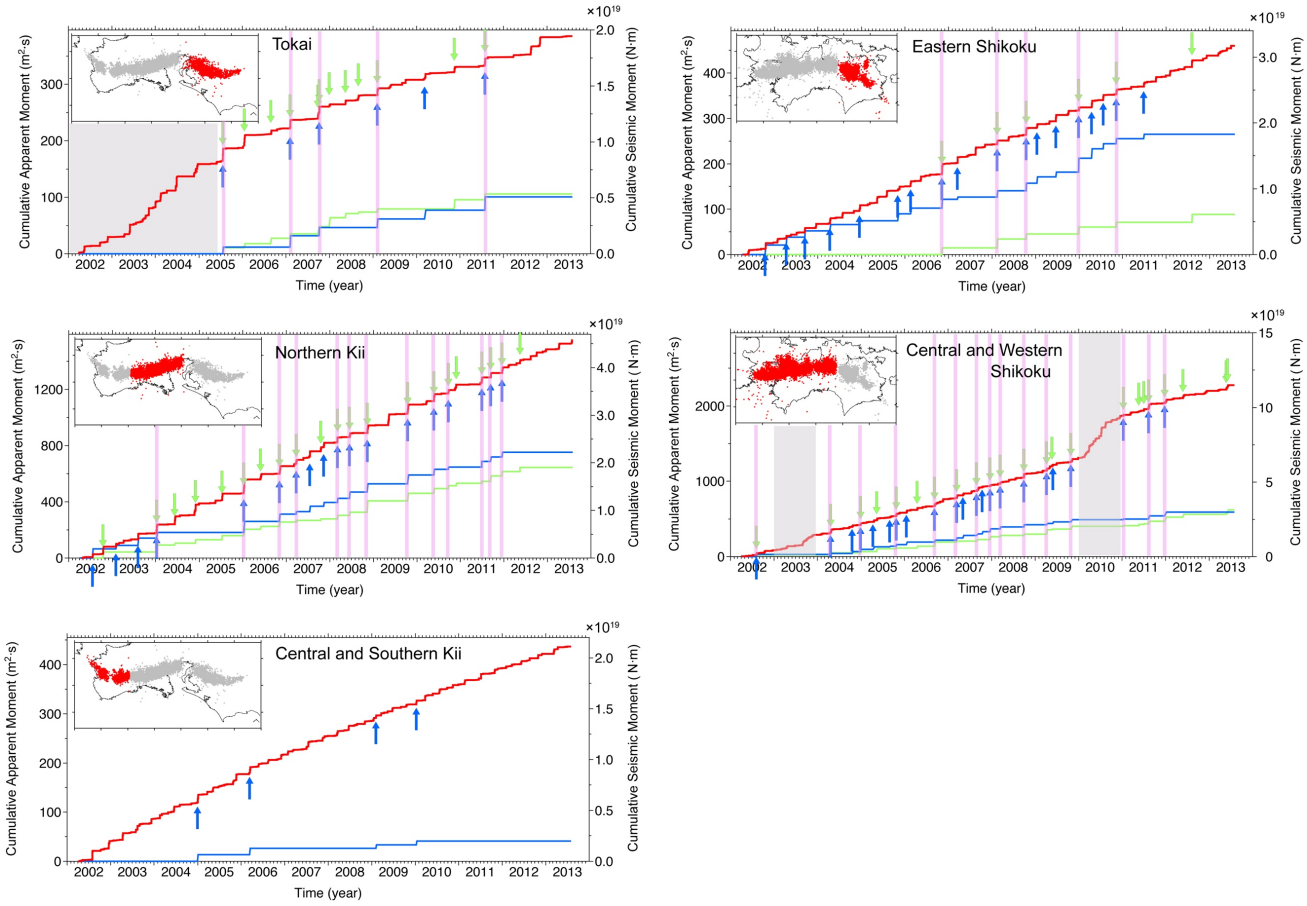

639

640 Figure 3.

641

642

643

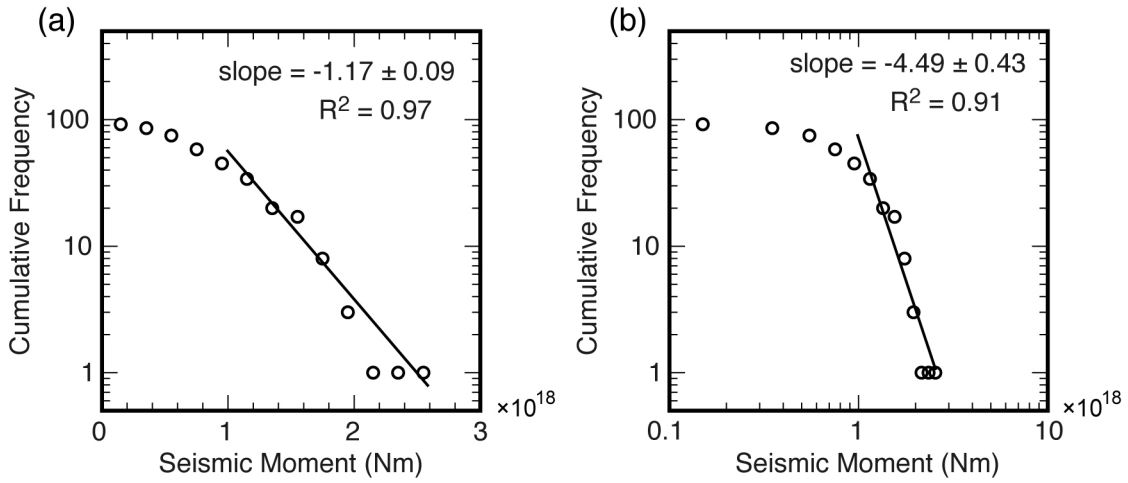

644

645

646 Figure 4.

647

648

649

650

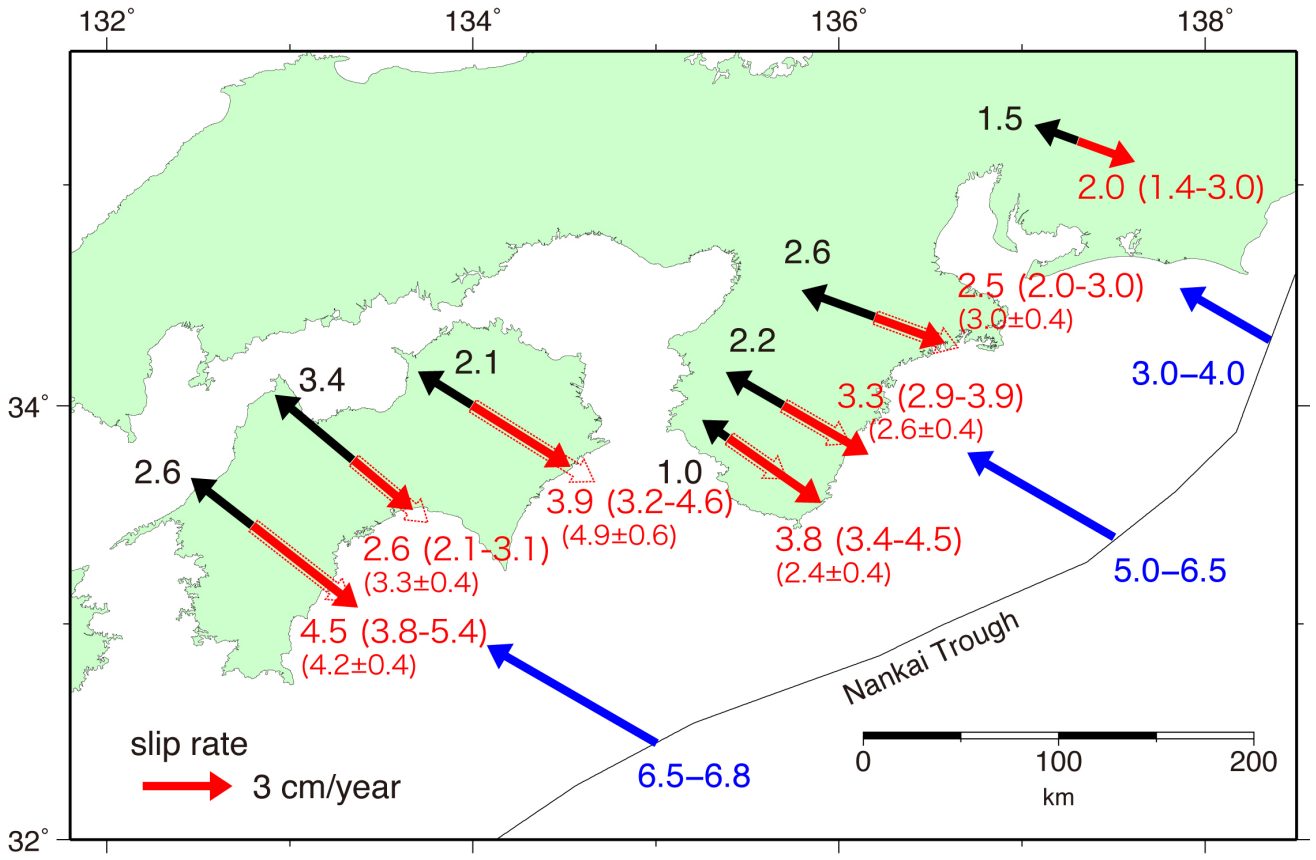

651

652

653 Figure 5.

654

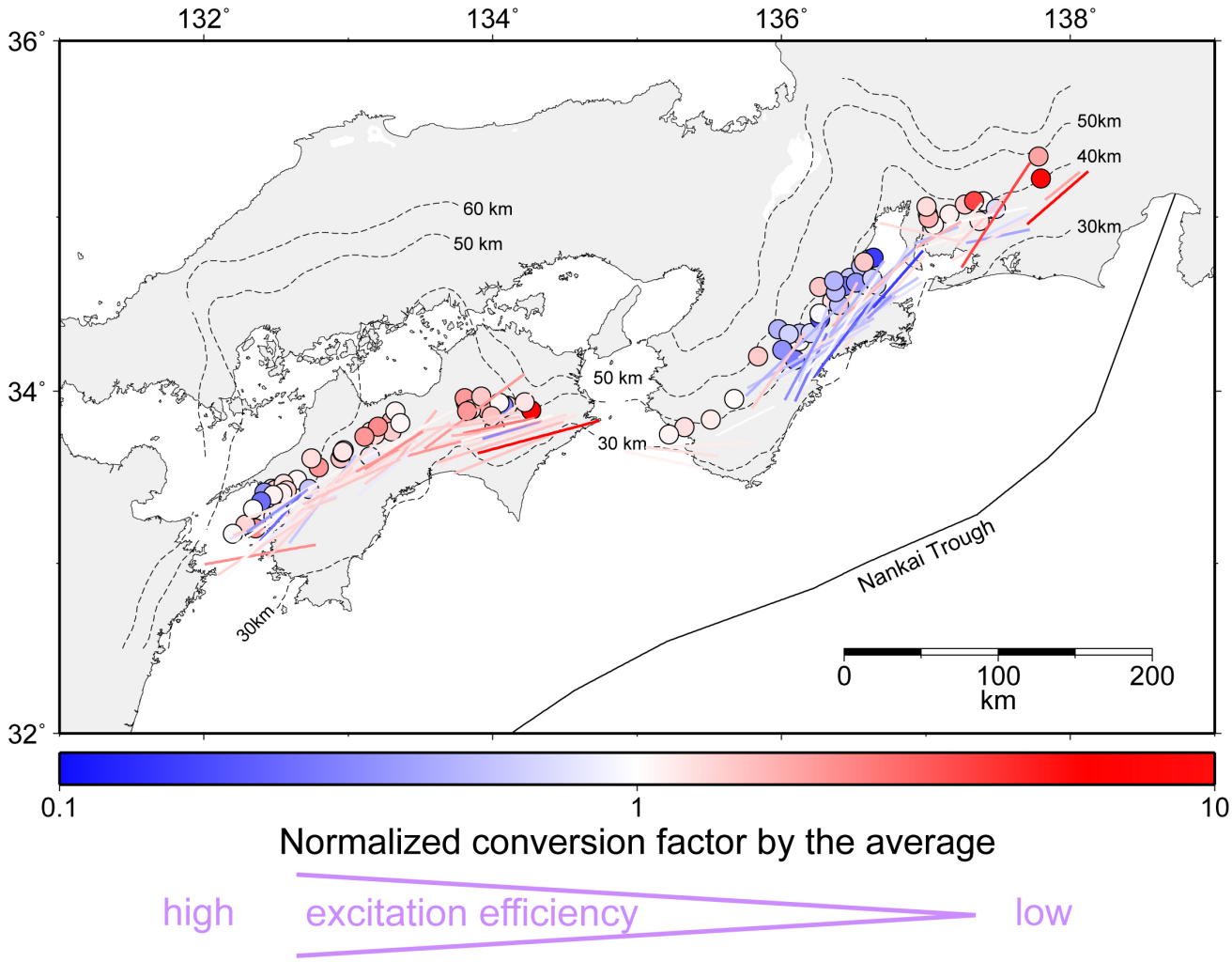
132˚
134˚
136˚
138˚
36˚
34˚
32˚
60 km
50 km
50 km
30 km
50km
40km
30km
30km
Nankai Trough
0
100
km
200
0.1
1
10
Normalized conversion factor by the average
high
excitation efficiency
low

Figure 6.

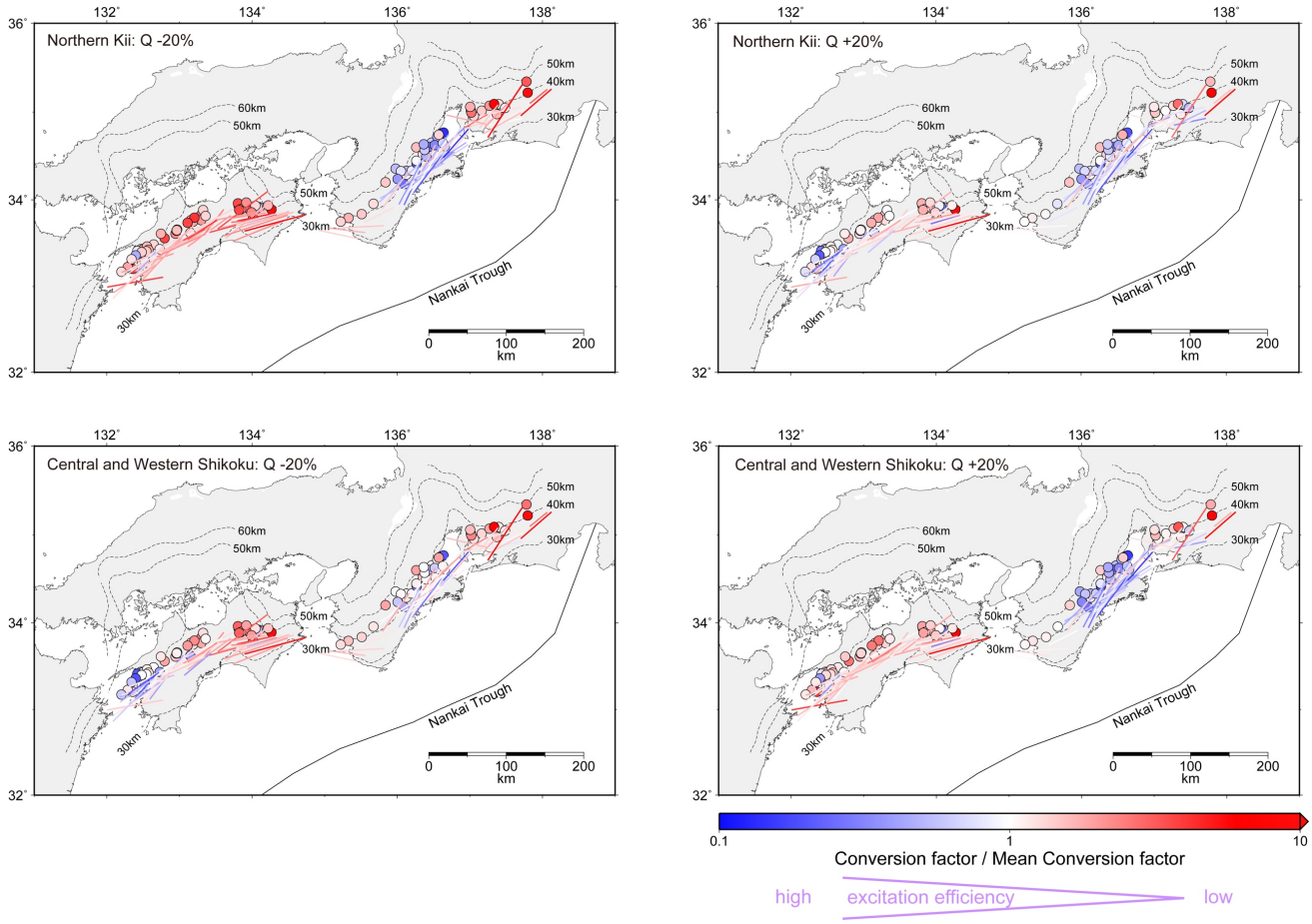
Northern Kii: Q -20%
Northern Kii: Q +20%
Central and Western Shikoku: Q -20%
Central and Western Shikoku: Q +20%
132°
134°
136°
138°
36°
34°
32°
50km
40km
30km
60km
Nankai Trough
0
100
km
200
0.1
1
10
Conversion factor / Mean Conversion factor
high
excitation efficiency
low

Figure 7.

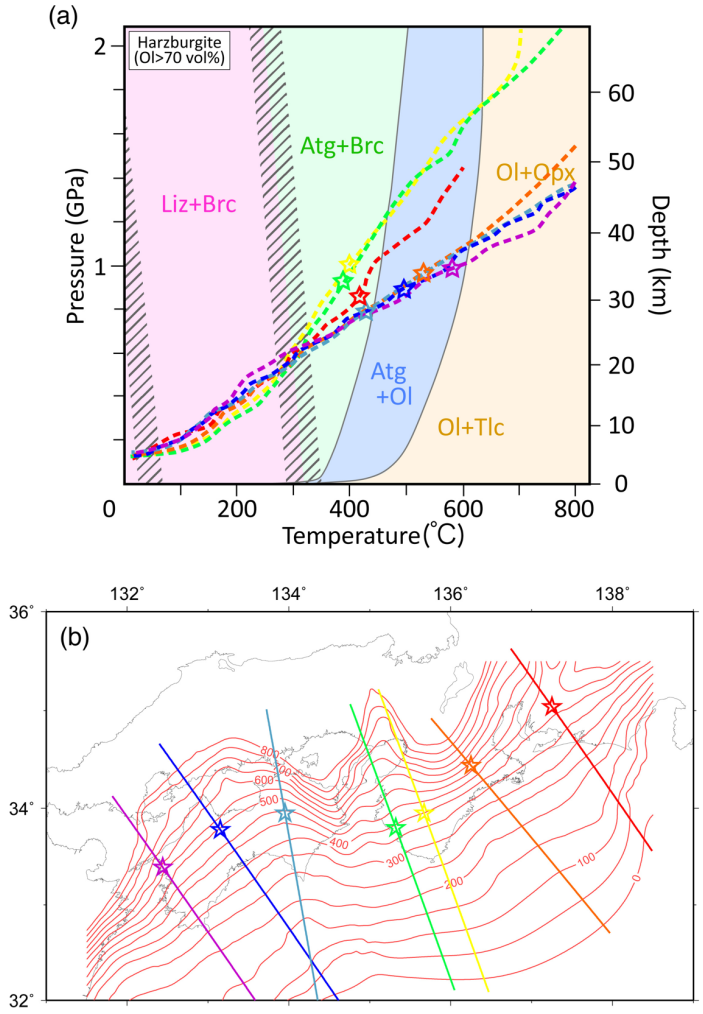
(a)
Harzburgite
(Ol>70 vol%)
Liz+Brc
Atg+Brc
Atg
+Ol
Ol+Opx
Ol+Tlc
Pressure (GPa)
Depth (km)
Temperature(°C)
(b)

Figure 8.

	SSE from both tiltmeter and GNSS	SSE from tiltmeter	SSE from GNSS
Tokai	5	7	1
northern Kii	13	8	5
central and southern Kii	-	-	4
eastern Shikoku	5	1	13
central and western Shikoku	15	8	7

Table 1.

	conversion factor (10^{16} N/m/s)	moment release rate (10^{18} Nm/yr)	fault area (10^{9} m^2)	slip rate (cm/yr)	convergence rate (cm/yr)	slip deficit rate (cm/yr)	convergence rate - slip deficit rate (cm/yr)
Tokai	5.3 ± 1.1 (3.7-8.1)	1.5 ± 0.3 (1.0-2.2)	1.8	2.0 ± 0.4 (1.4-3.0)	3.0 - 4.0[a]	1.5[b]	1.5 - 2.5
northern Kii	3.0 ± 0.3 (2.5-3.7)	3.1 ± 0.3 (2.5-3.8)	3.1	2.5 ± 0.3 (2.0-3.0)	5.0 - 6.5[a]	2.6[c]	2.4 - 3.9
central Kii	4.9 ± 0.4 (4.4-5.8)	1.1 ± 0.1 (1.0-1.3)	0.8	3.3 ± 0.3 (2.9-3.9)	5.0 - 6.5[a]	2.2[c]	2.8 - 4.3
southern Kii	4.9 ± 0.4 (4.4-5.8)	0.8 ± 0.1 (0.7-1.0)	0.5	3.8 ± 0.3 (3.4-4.5)	5.0 - 6.5[a]	1.0[c]	4.0 - 5.5
eastern Shikoku	7.0 ± 0.7 (5.8-8.4)	2.8 ± 0.3 (2.4-3.4)	1.8	3.9 ± 0.4 (3.2-4.6)	6.5 - 6.8[a]	2.1[d]	4.4 - 4.7
central Shikoku	5.1 ± 0.5 (4.2-6.1)	1.5 ± 0.1 (1.3-1.8)	1.5	2.6 ± 0.2 (2.1-3.1)	6.5 - 6.8[a]	3.4[d]	3.1 - 3.4
western Shikoku	5.1 ± 0.5 (4.2-6.1)	6.7 ± 0.6 (5.6-7.9)	3.7	4.5 ± 0.4 (3.8-5.4)	6.5 - 6.8[a]	2.6[d]	3.9 - 4.2

[a]Data from Miyazaki and Heki (2001), [b]Data from Suito and Ozawa (2009), [c]Data from Kobayashi et al. (2006), [d]Data from Tabei et al. (2007).

Table 2